A light-weight compact proton gantry design with a novel dose delivery system for broad-energetic laser-accelerated beams

Masood, U.; Cowan, T. E.; Enghardt, W.; Hofmann, K. M.; Karsch, L.; Kroll, F.; Schramm, U.; Wilkens, J. J.; Pawelke, J.;

Originally published:

June 2017

Physics in Medicine and Biology 62(2017)13, 5531-5555

DOI: https://doi.org/10.1088/1361-6560/aa7124

PMB manuscript No.

A light-weight compact proton gantry design with a novel dose delivery system for broad-energetic laser-accelerated beams

U. Masood[1*], T. E. Cowan[2,3], W. Enghardt[1,4,5,6], K. M. Hofmann[7,8], L. Karsch[1], F. Kroll[2], U. Schramm[2,3], J. J. Wilkens[7,8], J. Pawelke[1,2]

[1] OncoRay-National Center for Radiation Research in Oncology, Faculty of Medicine and University Hospital Carl Gustav Carus, Technische Universität Dresden, Fetscherstrasse 74, PF 41, 01307 Dresden, Germany

[2] Institute of Radiation Physics, Helmholtz-Zentrum Dresden-Rossendorf, Bautzner Landstrasse 400, 01328 Dresden, Germany

[3] Technische Universität Dresden, 01069 Dresden, Germany

[4] Institute of Radiooncology, Helmholtz-Zentrum Dresden-Rossendorf, Bautzner Landstrasse 400, 01328 Dresden, Germany

[5] Department of Radiation Oncology, Faculty of Medicine and University Hospital Carl Gustav Carus, Technische Universität Dresden, Fetscherstrasse 74, PF 41, 01307 Dresden, Germany

[6] German Cancer Consortium (DKTK), Dresden, Germany

[7] Department of Radiation Oncology, Technical University of Munich, Klinikum rechts der Isar, Ismaninger Str. 22, 81675 München, Germany

[8] Physics Department, Technical University of Munich, James-Franck-Str. 1, 85748 Garching, Germany

Abstract

Proton beams provide superior dose-conformity in radiation therapy. However, the large sizes and costs limit the widespread use of proton therapy (PT). The recent progress in proton acceleration via high-power laser systems has made it a compelling alternative to conventional accelerators, as it could potentially reduce the overall size and cost of the PT facilities. However, the laser-accelerated beams exhibit different characteristics than conventionally accelerated beams, i.e. very intense proton bunches with large divergences and broad-energy spectra. For the application of laser-driven beams in PT, new solutions for beam transport, such as beam capture, integrated energy selection, beam shaping and delivery system are required due to due to the specific beam parameters. The generation of these beams are limited by the low repetition rate of high-power lasers and this limitation would require alternative solutions for tumour irradiation which can efficiently utilize the available high proton fluence and broad-energy spectra per proton bunch to keep treatment times short. This demands new dose delivery system and irradiation field formation schemes. In this paper, we present a multi-functional light-weight and compact proton gantry design based on iron-less pulsed high-field magnets for laser-driven sources. This achromatic design includes an improved beam capturing and energy selection system, with a novel beam shaping and dose delivery system, so-called ELPIS. ELPIS system utilizes magnetic fields, instead of physical scatterers, for broadening the spot-size of broad-energetic beams while capable of simultaneously scanning them in lateral directions. To investigate the clinical feasibility of this gantry design, we conducted a treatment planning study with a 3D treatment planning system augmented for the pulsed beams with optimizable broad-energetic widths and selectable beam spot sizes. High quality treatment plans could be achieved with such unconventional beam parameters, deliverable via the presented gantry and ELPIS dose delivery system. The conventional PT gantries are huge and require large space for the gantry to rotate the beam around the patient, which could be reduced up to 4 times with the presented pulse powered gantry system. With the development of next generation high-power laser systems, with petawatt laser power, necessary to reach proton energies required for therapy application, it could be possible to reduce the footprint of the PT facilities, without compromising on clinical standards.

1 Introduction

1.1 Motivation

In radiation therapy, proton beams are able to provide numerous advantages compared to the state-of-the-art photon beam therapy because of their characteristic inverse depth dose profile, i.e. Bragg peak. These

*Corresponding author: e-mail: u.masood@hzdr.de, Phone:+49 351 260 3552, Fax:+49 351 260 13293

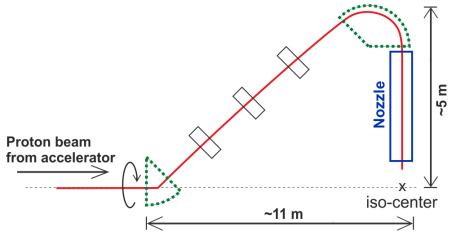

Figure 1: Figure represents a schematic layout of a conventional proton gantry. The mono-energetic pencil beam (red line) from the accelerator is transported, via magnetic transferlines, to the gantry. In the gantry, the beam can be rotated around the isocentre via dipole sector magnets (shown in green dotted line) while beam properties are maintained via magnetic quadrupoles (black rectangles). It is indispensable to shape or scan the mono-energetic pencil beam for patient irradiation with 3D tumour conform dose delivery. This beam shaping or scanning is done via beam delivery equipment, commonly known as nozzle, which is installed usually behind the last bend in the commercially available proton gantries. There are two basic beam delivery schemes are being used in conventional systems, namely passive beam scattering and active pencil beam scanning, see figure 2 for details.

advantages include superior dose conformity around tumour volumes, better sparing surrounding healthy tissues and organs at risk [1,2] and may reduce lifetime attributable risks of radiation treatment [3]. In proton therapy (PT) systems, proton beams are accelerated to therapeutic energies, i.e. 70-250 MeV, via the conventional synchrotrons or more commonly fixed energy cyclotrons with energy degraders and energy selection systems following the accelerator [4, 5]. The monoenergetic proton beam of a selected energy is then transported via magnetic beamlines to the treatment room, preferably, with a gantry system. A gantry, i.e. rotatable beamline system, is capable to rotate the beam around an isocentre in the treatment room to irradiate the tumour volume from different directions without moving the patient (see figure 1). However, high energy protons are rigid to bend, and with the conventional iron-core magnets (with maximum magnetic field strength of about 2 T) the isocentric proton gantries are massive (>150 tons) and large (up to ~11 m in diameter and ~11 m in length), e.g. see ref. [6]. Also, heavy support structures are required to rotate these gantries and are housed in enormous radiation protected buildings, which all adds up to the complexity and cost of PT facilities. The huge capital investment of about 25 - 100 million Euros (depending on the number of gantries), is the primary reason limiting PT to only about 50 operational centres worldwide [7]. Huge efforts are going on to reduce the footprint of the PT facilities as well as the costs by exploring both new acceleration schemes and new gantry designs, e.g. see references [8–12]. We explore the possibility to utilize laser-accelerated proton (LAP) sources and design a new compact gantry and dose delivery system based on light-weight high-field pulsed magnets.

1.2 Laser-accelerated protons

Recently, the rapid progress in the field of laser-driven proton acceleration has attracted interest in the medical and laser communities for its potential to facilitate a more compact and lower cost PT facility [10,13–16]. In laser-driven acceleration, a highly focused high-power laser pulse (with peak light intensity of 10^{19} W cm^{-2} or higher) interacts with matter (laser target) and accelerates protons on μm scale. The electro-magnetic field of the laser pulse initially generates plasma and accelerates electrons in the laser target. This creates charge separation, generating a quasi-static acceleration field, of the order of TV/m, accelerating preferably protons due to the highest charge-to-mass ratio. Protons with maximum energies of up to 90 MeV [17, 18] have been experimentally observed via 100 terawatt (10^{14} W) class laser-driven accelerators. Although, the generation and reproducibility of LAP beams, for full therapeutic energy range, are still to be established, the scaling models predict higher energies are reachable with increased laser power [19] and/or with new laser target geometries [20–22]. The development of the next generation petawatt (10^{15} W) laser systems [16, 23] promises the prospects of laser-driven PT in near future.

However, the LAP bunches exhibit very different beam properties than beams from conventional accelerators, i.e. they are ultra-intense proton bunches of picosecond pulse duration, with about 10^{12} protons per bunch [10,18] and with up to 10^4 times better beam emittances [24], however, have broad-energy spread (up to 100 %) and large divergence angles (~5-10°), and can be delivered with only low repetition rate of up to 10 Hz (this limit comes from the high-power laser systems). On the other hand, conventional beams are quasi-continuous

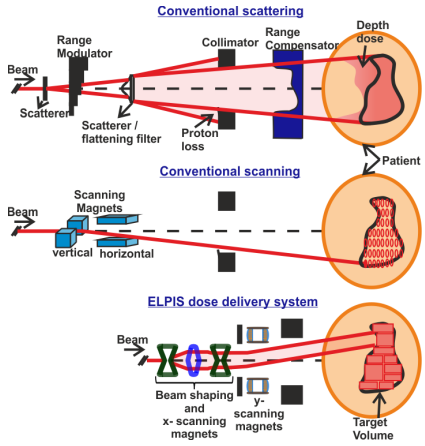

Figure 2: Schematic layout of the beam delivery approaches, comparing the two conventional approaches, passive beam scattering (top) and active pencil beam scanning (middle) (for more details see ref [25]), along with the new ELPIS system (bottom). In the scattering approach, the mono-energetic pencil-like proton beam is broadened laterally by physical scatterers and axially by modulating the energy spectrum via traversing through range modulator and patient specific hardware, such as collimators and range compensator, downstream to match the individual 3D tumour volume. This scheme is simple to implement and verify, as well as more robust in treating moving targets, however, limits the physical benefits of proton therapy because of the high doses to the healthy tissue volume in proximal region and also, it is only about 10% efficient due to the unavoidable proton loss in scatters, range modulator, compensator and collimators which results in secondary radiation close to the patient. The disadvantages of passive beam shaping are overcame by modern beam scanning option, in which a mono-energetic pencil-like beam is laterally scanned in combination with adapting the penetration depth by varying the beam energy delivered by the accelerator (like synchrotron) or selected by the energy selection system/range modulator (in case of cyclotron). Pencil beam scanning results in higher tumour conformity, however, with the beam spot-size of about 0.5 cm thousands of spots are needed to be irradiate to cover typical tumour volumes. Pencil beam scanning is more complex and it is more challenging to incorporate tumour motion, compared to scattering scheme. In conventional nozzles, it is not possible to combine beam scanning option with scattering, thus one cannot modulate beam size and position simultaneously, and also it requires a long time to switch between these two options. The advantages of both scattering and scanning schemes are combined in our new ELPIS system. The spectrally large proton beams can be spatially broadened via quadrupole magnetic fields, i.e. without the need to traverse through any physical material, while scanning the beam magnetically. The ELPIS system is explained in detail in section 2.4.4.

well-collimated (divergence $<0.2°$) mono-energetic ($\Delta E/E_o$ of $<1\,\%$) pencil beams. These particular properties make it challenging to adapt LAP beams directly for medical applications with existing PT equipment and dose delivery approaches. LAP beams require new optimized transport beamline solutions to control and utilize these specific beam parameters for efficient and precise dose delivery to match clinical standards.

1.3 Status and overview

The first attempt to design a gantry for laser-driven sources [26, 27] used a simple very low acceptance beamline with an aperture to limit the initial divergence for transport and a magnetic chicane approach for energy filtering of the LAP beams. For the final dose delivery to the patient, a beam scanning via whole beamline movement was introduced, in contrast to the prevailing use of magnetic fields. The precise motion of the massive laser target assembly, along with the magnetic energy selection system, for accurate scanning of about $20\times20\,\mathrm{cm}^2$ field size through pencil-like beams of about 1 cm spot-size would put critical mechanical constraints. Furthermore, the low acceptance of the energy selection system resulted in beam transport efficiencies of the order of $0.01\,\%$ [28, 29]. An alternative approach for the beamline was presented recently based on high-field pulsed magnets [30]. This design had advanced features like a large acceptance particle capturing lens and integrated energy selection system, so-called ISESS. This beamline showed the possibility to select and transport variable broad-energetic beams in a more robust gantry formation, with up to 22% transport efficiency. Also, for an overall compact gantry design, high-field pulsed magnets have been introduced which are much lighter and smaller in size than conventional iron-core magnets and can provide up to 5 times higher magnetic field strengths, synchronized with traversing pulsed LAP bunches. However, for highly tumour conformal dose delivery, it is necessary to shape or scan the beam via specialized equipment (please see upper and middle panel of figure 2). Such dose delivery system was not included in the gantry [30] because of the fact that beams with broad-energy spectrum chromatically diverge in magnetic fields used for beam scanning. Therefore, it was assumed that tumour coverage could be provided via patient-table movement with respect to the beam position. This design resulted in beams with limited control, and because of the table movement for tumour scanning, it

was not a clinically very attractive solution.

Thus, an improved rotatable gantry design is needed to control, shape and scan broad-energetic beams for efficient transport and tumour conformal dose delivery. In this paper, we present a new gantry improving the previous design (cf. [30]) by a two step beam capturing system and simplified energy selection system, ISESS. Additionally, for efficient and precise dose delivery a novel broad-Energetic Large acceptance beam delivery via magnetic field shaPing, Integrated with short-throw Scanning (ELPIS) system is designed and included. The ELPIS system can magnetically vary the spot-size of the beam and scan through a large irradiation field simultaneously. Also, it discards the use of physical elements, such as scatterers, modulators and range-compensators. This can improve the beam delivery efficiency and potentially reduce secondary radiation. Furthermore, for medical applications, it is crucial to establish the functionality for any new equipment or design on the basis of clinically relevant parameters. Therefore, we utilized a 3D treatment planning system (TPS), called LAP-CERR, which is capable to calculate treatment plans for broad-energetic pulsed laser-driven proton beams on 3D patient data(for details please see reference [31]). LAP-CERR was adapted for the specific beam features of the laser-driven protons source and the gantry output parameters derived in this paper. We present one clinical case as an example to demonstrate in principle the functionality of the improved gantry features by achieving treatment plans of high quality comparable to the conventional PT standards.

2 Materials and Methods

2.1 Laser-driven proton source

Although, the best understood laser acceleration mechanism is target normal sheath acceleration [32], there are other mechanisms under investigation [33–37] to improve beam quality. For example, radiation pressure acceleration mechanism could achieve up to 40 times increased laser to particle energy conversion efficiency than the robust target normal sheath acceleration regime [38] with improved beam parameters, like less initial divergence and energy spread.

However, to design and investigate a gantry, it is not necessary to consider a specific laser acceleration mechanism and to have pre-determined beam properties. A broad set of characteristic parameters can be defined for the design study and a robust design would than has the flexibility for optimization once experimental data is known. Target normal sheath acceleration type exponential beam energy spectra can also be employed here (as in reference [30]) and will not effect the qualitative results. However, we have assumed characteristic beam parameters of radiation pressure acceleration regime following the medical application studies of LAP beams by Hofmann et. al. [39, 40]. The beam spectral intensity distribution is described, in the ref. [40], as a bi-Gaussian

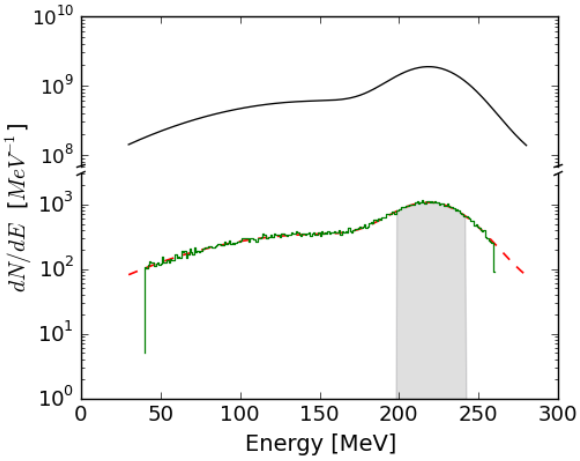

Figure 3: The blue line represents a predicted initial energy spectrum following eq. 1, the red line shows the same spectrum scaled down by a factor of 1.75×10^{6}, which was then used to generate proton bunches via a Monte-Carlo code, shown by green line. This reduction is made to save simulation time and computational power in tracking simulations. The shaded area represents protons in the $\Delta E/E_o = 20\,\%$ energy width, with peak at E_o=220 MeV, which as an example here were selected to be captured and transported via the gantry.

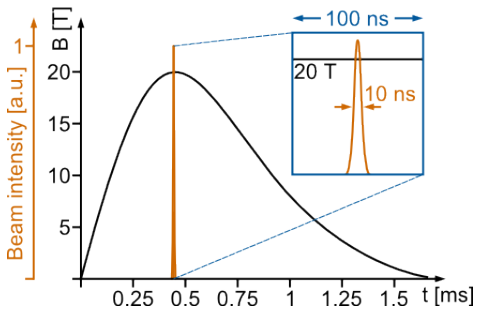

Figure 4: The figure shows (in black line) the magnetic field inside a pulsed magnet as a function of time. The rise time for the magnetic field usually ranges between 0.2-0.7 msec, depending upon the magnet type. However, the LAP bunch (orange line) traversing through the magnet only require propagation time in nsec scale. The magnetic field can be considered as uniform and static during the passage of the LAP bunch, as shown in the blown part of the figure.

fit to the simulated results and described as below:

$$N(E) = N_o[e^{-((E-E_o)/30)^2} + 0.4 \times e^{-((E-(E_o-70))/100)^2}] \quad (1)$$

It is assumed that peak energy E_o can be adjustable via laser parameters, i.e. laser intensity on laser target. Although, maximum number of protons are squeezed around the E_o, nevertheless, $N(E)$ contains protons with wide range of energies, see figure 3, and an energy selection system is still necessary. A Monte-Carlo code was written to generate proton bunches with spectral intensity distribution following eq. 1, with randomly distributed space and momentum coordinates (x, y, z, p_x, p_y, p_z) within the bunch, with maximum spot-size of $5\,\mu m$ and with maximum divergence of 75 mrad (~4.3°). These proton bunches were then used in the particle tracking simulations to mimic a laser-driven source.

2.2 Pulsed magnets

The pulsed structure of the LAP beams allows to utilize high-field pulsed magnets for a compact design. The magnetic rigidity ($B\rho = p/q$, where p is the momentum and q is the charge) of the protons with therapeutic energies require high magnetic field strength B for small bending radius ρ, which predominantly determines the size of any PT gantry. In conventional systems, room temperature iron-core magnets are being used in which the maximum magnetic field strength B_{max} achievable is limited, due to the saturation of the magnetization of the iron-core, to a value of $\leq$2 T. On the other hand, pulsed magnets have air-core and thick current carrying wires which are specially designed to shape a specific magnetic field region of interest. Electrical energy is supplied by high-power capacitor-banks. By eliminating the core-saturation limitation, B_{max} achievable with pulsed magnets is mainly limited by the peak current provided and the mechanical stability of the magnet structure. The pulse duration of the magnetic field inside pulsed magnets is of few milliseconds, however, it can be considered uniform for the traversing LAP bunches of up to few nanoseconds of length, see figure 4. The feasibility of pulsed magnets as capturing and focusing lenses (e.g. solenoid) for LAP bunches has already been demonstrated in many experiments [41–43]. Also pulsed dipole sector magnet [44, 45] and quadrupole magnet [46] are being developed. From our experience, we have considered moderate field strengths of $\leq$9 T for dipole fields and of $\leq$40 T for solenoidal fields as well as field gradient g_q <150 T/m for quadrupoles, and we use these values as the upper limit for calculating the gantry beamline.

2.3 Requirements from the gantry system

The LAP beams observe initial parameters, like, large energy spread and ~20 times larger beam divergences, and demand a large acceptance transport beamline system with multiple functionalities. The first function, is to capture the LAP and to control the intrinsic large divergences while keeping the beam small in transverse dimensions. This capturing function is necessary for maximum beam transport efficiency [39,40] and controlling the beam downstream. As a second function, an energy selection system is needed to filter and utilize the broad-energetic spectrum of LAP bunch generated by a laser pulse, or so-called shot. One crucial point is to keep

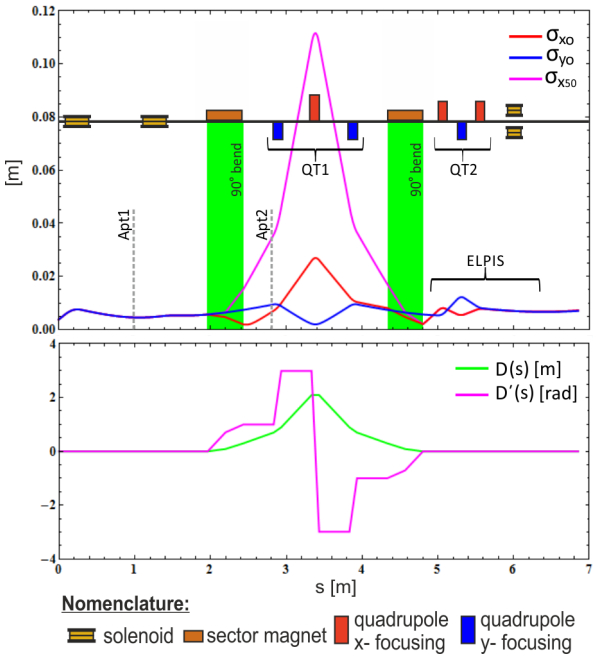

Figure 5: The gantry model (as explained in section 2.4) is graphically shown. The magnetic elements are drawn along the path length, as used in the model to manipulate the beam properties. The plot on top shows the beam envelopes, red and blue lines represent beam of protons with nominal energy and the magenta line represents the beam with 50 % momentum spread. The bottom plot shows the evolution of dispersion functions along the beamline in the default settings, i.e. with parallel beam at the isocentre without scanning. These plots change slightly with scanning option, see figure 11. This model is then translated in the particle tracing simulation code, please see figure 6 for corresponding magnet positions on particle tracks.

treatment times short in spite of the low shot (LAP bunch) repetition rate. The idea is to filter the LAP bunches for specific energy-widths to deposit doses simultaneously inside several spots (or sub-volumes), i.e. in axial direction (in-depth) by selecting optimal energy-width per laser shot, and laterally by varying the transverse size of the beam spot (see figure 2). For this reason, we design the system to select and transport up to 20 times broader energy width and up to 20 times larger variable spot-sizes, than conventional beams. This demands the third functionality of the beamline, that is to vary the beam spot-sizes for each shot to a value optimized in the TPS. The last function of the beamline is to deliver doses to the tumour volume with high precision and accuracy. In most of the conventional systems, dose delivery is done by specialized equipment inside the nozzle (figure 1). However, that is designed for fixed sized mono-energetic pencil beams. A new dose delivery and irradiation field formation system is needed to control and implement LAP beams, which is intricate and complex to design. The whole beamline then should be achromatic and be arranged in a gantry formation to rotate these beams around an isocentre for multi-directional tumour irradiation. The design and each function of the gantry is explained in the following section.

2.4 Gantry design

For the gantry design, an analytical model based on first order linear beam optics [47] has been developed (see figure 5 and 6 for the schematic setup). The initial parameters of the protons generated with the Monte-Carlo code could be defined by six-dimensional phase space $(x, x', y, y', L, \delta)$, where (x, y) and (x', y') are the transverse positions and slopes (flight directions) of the particles, with regard to the longitudinal beam axis z, respectively, and L is the bunch length (defined by bunch duration and proton energy) and $\delta = \Delta p/p_o$ momentum spread (which is directly related to the energy spread $\Delta E/E_o$). This 6D phase space is then used to determine the Twiss-parameters (α, β, γ), which statistically defined by the protons within the beam at any given position s along the beamline. A 6×6 matrix (M_o) can then be defined as follows to represent the initial beam:

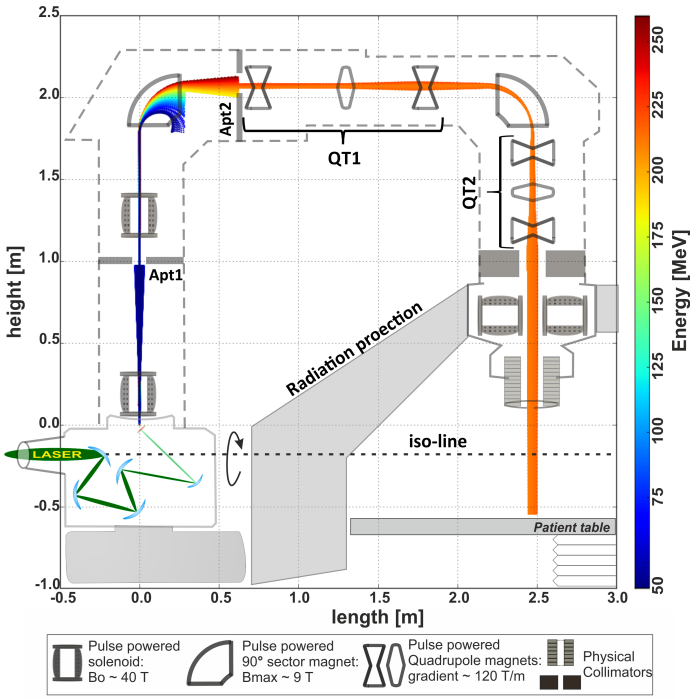

Figure 6: The figure shows the schematic design of the 360° rotatable gantry with laser target chamber and patient treatment site. For a compact arrangement, the idea is to transport laser pulses from the laser system directly into the gantry via optical lines in to an integrated rotatable laser target chamber, thus omitting the need of heavy magnetic transferlines between accelerator and gantry. Laser-pulses could be focused on the laser target (red 45 degree thin short line) generating LAP bunches, which are then captured, energy sorted and transported to the patient site. The proton tracks from the particle tracking simulations and the individual magnetic elements are drawn along the nominal path as described by the model, see figure 5. The size of the gantry is 2.4 m in radius and 3.4 m in length.

$$M_o = \begin{pmatrix} \epsilon_x\beta_x & -\epsilon_x\alpha_x & 0 & 0 & 0 & D(s) \\ -\epsilon_x\alpha_x & \epsilon_x\gamma_x & 0 & 0 & 0 & D'(s) \\ 0 & 0 & \epsilon_y\beta_y & -\epsilon_y\alpha_y & 0 & 0 \\ 0 & 0 & -\epsilon_y\alpha_y & \epsilon_y\gamma_y & 0 & 0 \\ 0 & 0 & 0 & 0 & L^2 & 0 \\ 0 & 0 & 0 & 0 & 0 & \delta^2 \end{pmatrix} \tag{2}$$

where, ϵ is the emittance of the beam, and $D(s)$ is the dispersion as a function of nominal path s and $D'(s)$ is the slope of the dispersion (further explained in section 2.4.2). The effect of each beamline element, i.e. solenoids, quadrupoles and dipoles, along with the drift spaces can also be written in 6×6 transfer-matrices. For a specific arrangement of magnetic elements, a combined sequence of these transfer-matrices (M_{BL}) can represent the gantry. The beam parameters (M) after traversing through a beamline, characterized by M_{BL}, can be determined by:

$$M = M_{BL} M_o M_{BL}^T \tag{3}$$

The magnetic field strengths needed for each beamline element were determined for desired beam properties at the isocentre. The intricacies of the mathematical solution has to satisfy multiple conditions simultaneously, e.g. beam capturing and collimating of large divergences at E_o, large dispersion for energy selection, acceptance constraints for large δ values, dispersion correction and achromaticity at the end, and preferably with low number of magnetic elements to keep the system compact and energy-efficient. This analytical model of the gantry (eq. 3) considers a hard-edge model for magnetic fields and it is important to simulate LAP beam traversing through the design to establish the functionality of the model. For this purpose, the General Particle Tracking (GPT) simulation package [48] was used and this gantry model was translated in GPT for tracking simulations. The main functions of the gantry are explained in detail below.

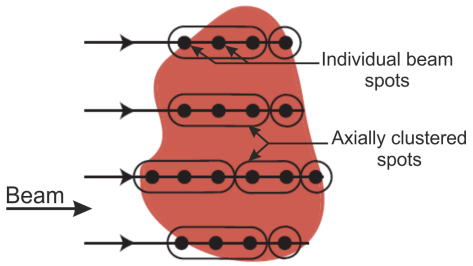

Figure 7: In conventional active scanning system, tumour volume is scanned sequentially with individual beams with fixed spot size. However, to reach a similar dose distribution several spots can be combined axially and irradiated simultaneously with one laser-shot with broad-energetic beam with specific energy window filtered by the energy selection system. This scheme is called axial clustering [31, 49] which maximizes the use of available proton number and energy spectrum, and ensures efficient treatment delivery.

2.4.1 Beam capturing and collimation

The LAP bunches require capturing due to the large initial divergences, to control and prevent losing the beam in to the beam-pipe. The capturing system must be efficient and capable to keep the beam small and collimated for the energy selection and further transport through the beamline. A single lens capturing, based on pulsed solenoid, has been investigated for gantry design [30, 40, 41], however, it provides limited control over the beam. We introduce an improved two step capturing and collimation system, based on two pulsed solenoids, for enhanced control of the beam. The first solenoid is positioned, with the beam entrance, at 2 cm downstream from the laser target and with an aperture of $\varnothing$ 2.5 cm. The diverging LAP bunch interacts with the solenoidal field which bends the protons symmetrically towards the central axis. The solenoid acts as a chromatic focusing lens with a focal length $f^{-1} = B_o^2 q^2 l / 4p_o^2$ (where l is the length of the solenoid and p_o is the momentum of the protons with nominal energy E_o). The magnetic field strength B_o is adjusted via provided current $I = 2GB_o/\mu n$ (where G is the geometric factor, μ is the permeability of the air-core and n is the number of windings per meter). A 4×40 windings solenoid structure was considered. The focusing strength of the capturing solenoid was adjusted for a minimum beam waist of 3 mm at 1 m downstream from the source position. At this focal-spot, an aperture (Apt1 in figure 5) was positioned to limit the proton energy spectra. Behind this point the beam starts to diverge again and a second solenoid, with the same geometry, was placed which re-captures and collimates the beam around E_o. In this way, the first solenoid can be optimized for maximum capture efficiency, by allowing maximum opening angle, independent of the second solenoid which was then optimized to deliver collimated beam with smaller transverse dimensions.

However, the second solenoid can only be optimized for collimating protons of energy E_o, the protons with $E > E_o$ experience less focusing-strength and protons with $E < E_o$ experience higher focusing-strength. Beams with large momentum spread δ values grow in size with drift length, which directly relates to large $\beta(s)$ values. The beam transverse phase-space was matched via the second solenoid for the acceptance ($A = r^2/\beta(s)$ [mm mrad], where r is the radius of the beampipe) of the dipole spectrometer (first 90° bending magnet) downstream for main energy selection and transport. But for the large δ beams, it is difficult to control Twiss-parameters for compact achromatic transport and furthermore, it is important to keep the radius r large for maximum transport efficiency, thus large magnetic field region, which would complicate the design requirements for the downstream pulsed magnets. Therefore, we considered a maximum value of $\Delta E/E_o = 20\,\%$ to be filtered and transported to the patient-site, which would be a good compromise between equipment design, beam control and transport, and for treatment dose delivery options.

2.4.2 Energy selection system

Laser-driven sources observe large energy spread and require an efficient energy selection system. A 90° dipole bending magnet is used which would provide two-fold functionality, i.e. beam energy selection and bending the beam. A gantry integrated shot-to-shot energy selection system (ISESS) was presented in reference [30] which included a 90° bending magnet in combination with a quadrupole-triplet. For this gantry design

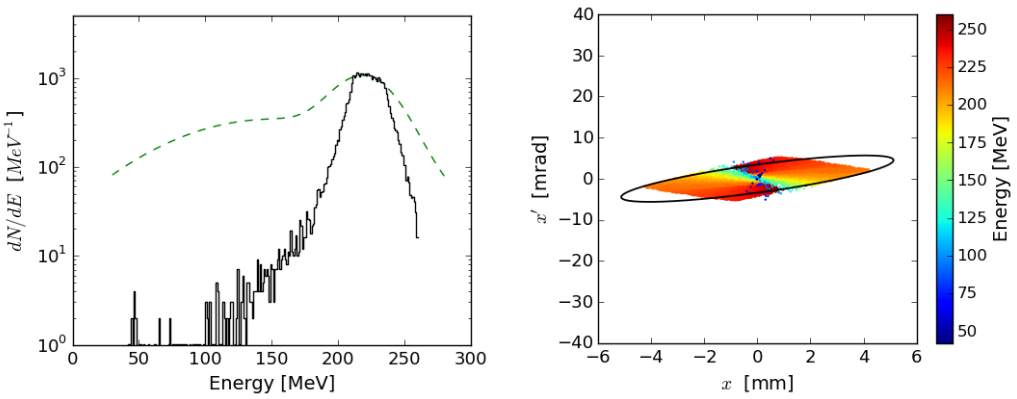

(a) (b)

Figure 8: In figure (a) the green dotted line shows the initial energy spectrum of a LAP bunch entering the gantry, the black line shows the spectrum after the capturing and collimation system for $E_o = 220\,\text{MeV}$, just before the first dipole sector magnet in figure 6. Figure (b) shows the corresponding particle distribution in the transverse phase space, while black ellipse represents the acceptance of the magnetic energy selection system downstream.

we have simplified the ISESS, by excluding the need of the extra set of three quadrupoles behind the dipole for energy selection, and could show that a similar energy selection resolution can be achieved with the well-collimated beams from the two-step capturing system.

The dispersion function, in eq. 2, introduced by the bending magnet in the beam, can be described as $D(s) = \Delta x/\delta$, where Δx is the distance of the mean position of the particles with Δp momentum difference from the ideal path. This energy dependent spatial spread provides the necessary condition for energy selection and the objective is to select δ (or $\Delta E/E_o$), as a function of the radius R_{apt2} of the principal energy selective aperture (Apt2) behind the bending-spectrometer, see figure 6. The energy resolution could be described as $\delta^{-1} = D(s = z_{apt2})/2R_{apt2}$, where $R_{apt2} = \sqrt{\epsilon\beta}$ is required to match the $\sigma = \sqrt{\epsilon\beta}$ of the beamlet with specific δ spread and emittance ϵ. The z_{apt2} is the position of the Apt2, which is chosen where $D(s)$ is relatively large and σ is preferably equal in both x- and y- directions for efficient and symmetric energy filtering, see figure 5. The R_{apt2} could be varied for each shot which in turn determines the energy width filtered from the initial spectrum. Also, it is important to define the transport efficiency, $\eta(E_o)$, as the system is optimized to deliver only a certain energy window of interest around a selected E_o per shot out of the initial spectrum. We define it as percentage ratio of transported number of protons in 1 MeV energy band around E_o and initial number of protons in the same band. This is a simpler definition independent of the initial and filtered $N(E)$ distribution shapes.

2.4.3 Beam transport

For a homogenous beam profile at the isocentre, it is crucial to cancel the dispersion functions, $D(s)$ and $D'(s)$, introduced by the ISESS 90° bending magnet. This requires beam control via magnetic quadrupoles. A set of quadrupole triplet (QT1) is introduced to control the spatially resolved beam. A second 90° bending magnet is necessary to bend the beam towards the patient-site, and thus form a rotatable isocentric gantry formation. The drift spaces and the individual strengths of QT1 quadrupoles were calculated by solving eq. 3 for $D(s) = 0$ and $D'(s) = 0$ (called as double-achromatic condition). The beamline parameters are also optimized to keep the beam small in transverse dimensions before the beam shaping and dose delivery system behind the second bending magnet, see figure 5 and 6. At this point, the beam is required to be spatially shaped according to the tumour dimensions to deliver the specific dose distribution pre-calculated by the 3D-TPS.

2.4.4 Beam delivery via ELPIS system

In clinical application, two basic techniques for beam delivery are being used in conventional systems, namely passive scattering and active beam scanning (please see figure 2 for description). These two schemes have been developed for continuous mono-energetic pencil-like beams from conventional accelerators. Both schemes have

specific advantages over the other, however, the equipment used in conventional nozzles does not allow to combine the two modalities for the modulation of the beam size and position simultaneously.

In principle, it is possible to use both conventional schemes for LAP beams, if mono-energetic spectrum is filtered out from the initial energy spectrum. A scattering system for LAP beams, with conventional components, will hugely reduce the efficiency in dose delivery given the low repetition rate (up to 10 Hz) and proton loss in physical materials. And if a conventional scanning system is to be considered for LAP beams, than the low repetition rate puts a critical constraint on treatment delivery time, as the time structure of magnetic fields and LAP bunch lengths does not allow to scan during one bunch.

A different dose delivery strategy is needed to efficiently use these specific properties, e.g. a specific broad-energy band filtered from the large initial energy spread can simultaneously deliver doses to several spots/slices in-depth of tumour volume (i.e. in axial direction) and the high number of protons ($\sim 10^{10-12}$ protons per bunch) can be spread over larger area (i.e. in lateral direction) by changing the spot size of the beam. Schell and Wilkens [49] presented three advanced dose schemes, in addition to conventional scattering and scanning options, namely axial clustering, lateral clustering and partial volume irradiation (which is the combination of the first two), and these schemes can reduce the number of scanning spots to be irradiated about half (please note the number of spots is not equal to the number of laser shots required to deliver the prescribed dose). However, there is a need to design an equipment to be able to shape and scan such broad-energetic large acceptance beams.

We present a new field formation and beam delivery system, so-called ELPIS, which is able to deliver above mentioned advanced dose schemes for simultaneous irradiation of multiple spots in both axial and lateral directions. ELPIS includes a quadrupole triplet (QT2) and horizontally arranged solenoid pair for the beam shaping and scanning technique. The beam optical imaging parameters of QT2 can be adjusted per LAP bunch so that the beam transverse size forms an uniform spot at the isocentre of selectable sizes. By selecting the peak energy E_o and energy width $\Delta E/E_o$ via ISESS and in transverse size via ELPIS, for each laser-shot, different unequal sub-volumes of the tumour can be irradiated, resulting conformal irradiation of the full extent of a tumour volume. Furthermore, beam shaping is performed without traversing through any physical material, which preserve proton fluence and reduce neutron generation.

Two separate approaches for beam scanning in lateral directions, i.e. x- and y-, are included in ELPIS. For scanning in x- direction, we utilize the fact that the offset in the quadrupole position with respect to the beam centre delivers a dipole-kick, which can be described as $\Delta x'_t = \frac{k_q \Delta x_c}{1+\delta}$ (where $k_q = g_q/(B\rho)$ is the normalized quadrupole strength and Δx_c is the offset in quadrupole position) [50], which are used to scan the beam. The quadrupole set QT2 is assumed to have mechanically controlled shifts $\pm\Delta x_c$. For beam scanning in y- direction, we utilize the bending term ($\vartheta \times B$) of the Lorentz-force by a dipole field generated in-between two pulsed solenoids. These two solenoids are arranged so that their apertures face each other, separated by a small gap and with the same direction of current. The beam traverses through the gap perpendicular to the axis of both

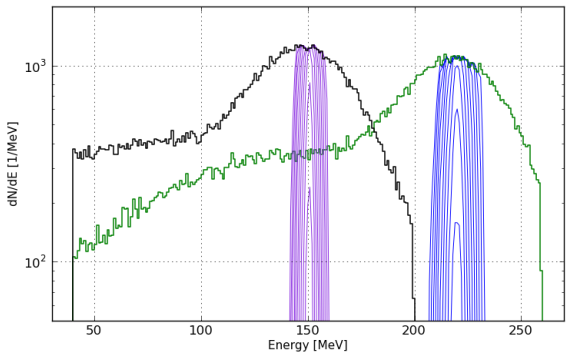

Figure 9: Energy spectra at the isocentre filtered through ISESS and transported via the gantry. The black and green spectra represent two exemplary LAP bunches with energy peaks at 150 MeV and 220 MeV respectively, as described by eq. 1 in section 2.1. The magenta and blue set of curves, under the respective black and green initial proton distributions, shows the filtered spectra transported for varied R_{apt2} values selecting energy widths between 3 % (inner line) and 19 % (outer line).

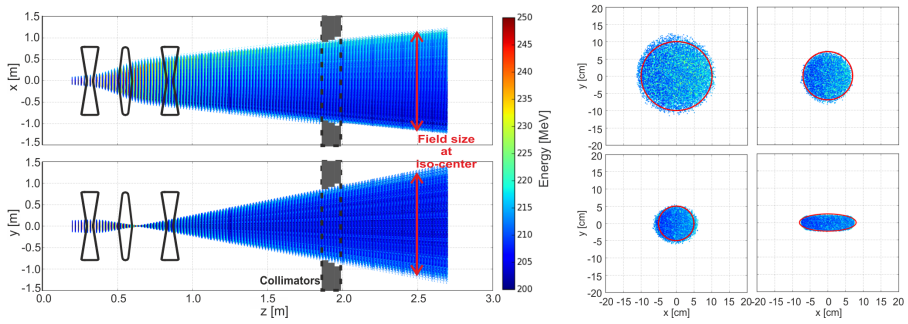

(a) (b)

Figure 10: Figure (a) shows the proton trajectories of a LAP bunch with $\Delta E/E_o$ 19 % at E_o = 220 MeV and represents the schematics of beam broadening via quadrupole set QT2 of the new dose delivery system, ELPIS. By changing the QT2 settings the beam spot-size and shape can be altered, figure (b) shows, as example, four beam spots at the isocentre for different QT2 settings.

solenoids and experiences a net bending force in y-direction. The bending angle is controlled via the current provided to the solenoids. At the end, before the exit-window of the gantry, a 6 cm thick collimator with variable aperture size, was used to prevent stray particles on the edges to pass through. This collimator is not used to shape the primary beam as in conventional passive scattering methods (see figure 10).

2.5 3D treatment planning system

Depending upon the beam delivery system in the gantry in conventional PT, there are two basic treatment delivery options available, namely passive scattering and active scanning approaches (see figure 2). Due to the better dose conformity and sparing of organs at risk the scanning option has advantages over the conventional scattering scheme. In this approach, a 3D TPS calculates dose distributions via a three-dimensional grid of beam spot positions, where each spot is irradiated with a different intensity and beam energy to cover the entire tumour volume for best possible dose conformity. A clinically relevant treatment plan requires a certain energy range to scan the entire extent in-depth of the tumour, which is delivered in pre-defined energy steps corresponding to a certain depth in the patient (see figure 7). Since the beam is scanned over the tumour volume in both lateral directions, there is no possibility to irradiate different adjacent spots simultaneously. However, with laser-driven protons having an intrinsic energy spread and by using the presented gantry and ELPIS dose delivery system, beams can be provided where various adjacent spots (laterally and/or in depth) can be irradiated with one laser shot.

For efficient use of such beams for tumour irradiation, a 3D-TPS called LAP-CERR capable to calculate dose distributions with pulsed broad-energetic proton beams has been developed [49] and its feasibility as a planning tool for laser-driven sources has been shown by Hofmann et al. [31]. The distinctive feature of LAP-CERR is that it can optimize dose distributions for the best tumour coverage and dose conformity on 3D patient data by combining several scanning spots axially and/or laterally to be irradiated simultaneously within one laser shot. These schemes are called axial clustering, lateral clustering and partial volume irradiation [49]. In this feasibility study we utilized axial clustering (see figure 7) with a fixed beam spot size and LAP-CERR optimized the best suitable energy widths and intensities per laser-shot required from the ISESS system (a detailed explanation of dose calculation and optimization of LAP-CERR can be found in [31]).

In order to test ELPIS and the presented gantry design, we have adapted LAP-CERR for the specific input source parameters (section 2.1) and the output results of the tracking simulations through the gantry, presented in section 3.1. As an example of our feasibility study a head and neck patient is shown, who was previously treated with high-energy x-rays at the Department of Radiation Oncology at Technical University of Munich, Germany. The LAP-CERR plans were analyzed on clinically relevant parameters like tumour coverage, $TC = \frac{V_{T,p}}{V_T}$ and the conformation number, $CN = \frac{V_{T,p}.V_{T,p}}{V_T.V_p}$, (for details see reference [51]) where: V_T is the target volume, V_p is the whole volume receiving at least the prescribed dose and $V_{T,p}$ is the target volume receiving at least the prescribed dose. With the help of these parameters as well as by the dose volume histograms it was ensured that the generated plans were similar to clinically accepted plans. Another important value in the

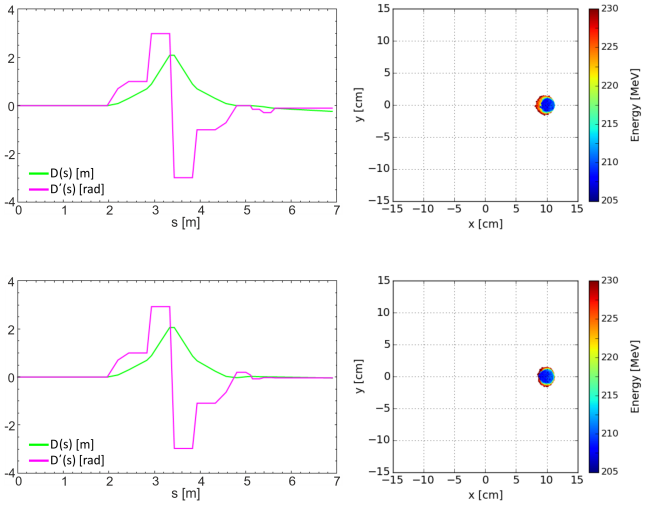

Figure 11: Dispersion plot (left) and the corresponding beam spot (right) for the scanned LAP beam with $E_o = 220\,\text{MeV}$ and $\Delta E/E_o = 19\,\%$ at the default gantry settings (top) and the beam spot after applied dispersion correction (bottom), as explained in section 2.4.4

evaluation is the number of laser-shots required to achieve the calculated treatment doses because this value determines the overall treatment time.

3 Results

3.1 Gantry design

For the design parameters of the gantry, we have solved eq. 3 for the conditions discussed in detail in section 2.4 with upper limits on the magnetic fields mentioned in section 2.2. Several solutions were obtained and tested with tracking simulations, however, as the optimized solution (see figure 6) we take drift lengths of 40 cm between quadrupole triplet QT1 and each of the two dipoles, with quadrupole lengths of 12 cm and normalized individual quadrupole strengths of $k_q < 6$. In the default settings, the QT2 parameters are set to deliver a parallel beam at the isocentre.

The gantry is designed for protons with maximum energy of 250 MeV, which corresponds to a magnetic rigidity of 2.43 Tm. The higher magnetic fields achievable by the pulsed magnets, in comparison to conventional magnets, result in smaller bending radii, i.e. a bending radius of 30 cm for the $B_{max} < 9\,\text{T}$ pulsed dipole sector magnets. Overall, we were able to reduce the size of our gantry to 2.4 m in radius and ~3.5 m in length which is about 2 times smaller in height and about 3 times shorter in length than most of the conventional isocentric gantries deployed in PT facilities.

To demonstrate the functionality of gantry design, the beam tracking simulation were performed with GPT. The capturing system provided a course energy filtering which prevented low energy tail of the spectrum to pass through, see figure 8 (a). For optimized capturing, a maximum magnetic field in the solenoids of 40 T was needed, which required currents up to 45 kA. An aperture (Apt1) with 1.8 mm fixed radius and 5 cm thickness at the focal-spot could efficiently cut the higher energy section of the spectrum, around the desired E_o, for further transport with above 99 % transport efficiency. The second solenoid recaptured and collimated the LAP bunch, as a typical example figure 8 shows the beam profile for $E_o = 220\,\text{MeV}$ before the ISESS bend.

The magnetic fields in the beamline sections following the beam capturing and collimation section (cf. figure 6) were calculated and tuned for the specific E_o in the full therapeutic range. The radius R_{apt2} of the energy selective aperture Apt2 was varied for filtering specific $\Delta E/E_o$ energy windows. The filtered $\Delta E/E_o$ windows could be selected ranging from 3-19 % in 1 % steps, see figure 9. The filtered bunch was then transported through the gantry and the spectra were measured at the isocentre. The transport efficiency $\eta(E_o)$ is different for each selected window, with decreasing efficiency for reducing the energy width. For the energy widths in the

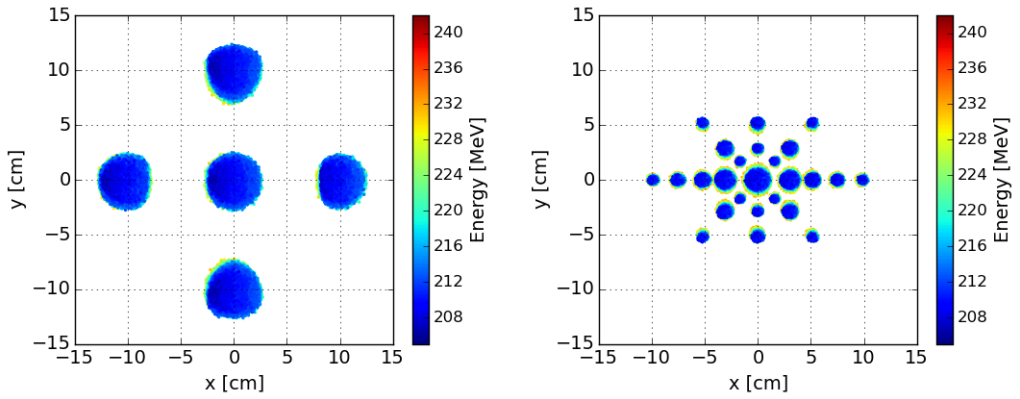

(a) (b)

Figure 12: Simulation results for the different beam sizes at the isocentre for different lateral beam positions. The beam parameters of $E_o = 220\,\text{MeV}$ and $\Delta E/E_o = 19\,\%$ were selected and transported via the gantry with the integrated ELPIS system. Figure (a) shows scanning of the large spot-size beams while figure (b) shows scanning of beams with varied smaller spot-sizes. The combination of different spot-sizes with different energy widths for different sub-volumes of a tumour would provide most efficient dose delivery without compromising tumour conformity.

range of 19-14 % the $\eta(E_o)$ is as high as 97 %, for the range 13-10 % the $\eta(E_o)$ decreases from 95 % to 70 %, and for the the range 9-3 % the $\eta(E_o)$ drops down to 20 %, which was expected as ISESS is not designed for high energy resolution but to select larger $\Delta E/E_o$ windows. The filtered energy spectra could be approximated by a higher order parabolic function: $N(E)_{filtered} = a(E - E_o)^6 + k$, where a was determined for each curve from the tracking simulations and k is related to $\eta(E_o)$. These curves were then used to create a library for the 3D TPS, LAP-CERR, to choose from.

3.2 Beam delivery via ELPIS system

To efficiently deliver a tumour conform dose distribution, the beam spot size and shape can be varied via QT2 settings. Figure 10 shows different spot-sizes in elliptical shapes achievable at the isocentre. The beam spot-size could be chosen from diameter 20 cm to 1 cm, see figure 12. In contrast to conventional systems, the fluence, however, cannot be kept constant because of squeezing the beam into different sizes and this needs to be taken into account by the TPS.

In the scanning magnets of ELPIS, about 5 times larger bending angles than conventional systems, could be achieved. Thus, short-throw scanning could be delivered without the need to increase the height of the gantry.

Nevertheless, due to the introduction of the dipole term by the scanning system, downstream to the QT2, the dispersion functions, $D(s)$ and $D'(s)$, became non-zero, which resulted in energy dispersion in the beam spot at the isocentre, see figure 11. A shot-to-shot dispersion correction technique was introduced to compensate the dispersion for each beam position in the scanning field. This was done by the adjustment in the QT1 parameters upstream so that the conditions $D(s) = 0$ and $D'(s) = 0$ are satisfied after including the effect of the scanning, see figure 11. As all magnets are assumed to be pulse powered at 10 Hz to match pulsed LAP beam, there is enough time to implement the shot-to-shot dispersion magnetic correction in between two LAP bunches and this would not complicate the pulsing system. However, the correction could only be applied in x-direction and the dispersion effect in y- direction needs to be accounted for either by the TPS or by restricting the scanning field to maximum size of 20×10 cm^2. The beam/dose delivery by the new ELPIS system can deliver large (selectable) spot-size beams with broad-energy windows and can scan in both lateral (x- and y-) directions, required by the advanced dose delivery schemes of lateral and axial clustering.

3.3 Treatment Plans

In order to show the clinical feasibility of the new gantry and the dose delivery system ELPIS, a treatment planning study was conducted, similar to the study by Hofmann et al. [31]. We utilized the axial clustering technique to compute a laser-driven proton plan for a head and neck cancer patient. A large tumour volume of

nearly 600 cm^3 was chosen. The 3D TPS LAP-CERR has been adapted for the output beam parameters of this improved gantry design. In particular, LAP-CERR was constrained to utilize nominal energies ranging from 50 to 250 MeV in 1 MeV steps and to select energy windows $\Delta E/E_o$ in the range of $3-19\,\%$ in $1\,\%$ steps (cf. section 3.2). Moreover, the transport efficiencies per selected energy window were implemented according to the simulation results. Beams with 2.0 cm FWHM spot-size were employed to deliver the dose via the active beam scanning option of the ELPIS system. Such a large spot size is not utilized in conventional proton therapy, however, it lead to a large reduction of the overall laser shot number while still leading to clinically relevant dose distributions.

The studied patient (see figure reffig:ptDose) was irradiated from two beam directions, namely 50 and 300 degrees, which represents a realistic clinical proton therapy scenario where usually 1-3 beams are utilized. The LAP bunches are intense sources, and with the improved transport efficiency of the gantry the delivered beams of 2 cm size still could reach much higher local doses than the prescribed dose for the tumour. Therefore, the fluence needed to be reduced in the TPS by a factor of 400 from the assumed initial proton number per bunch described in the section 2.1.

We found an optimal plan which would require 12326 laser-shots to treat this patient with a dose per fraction of 2 Gy. Assuming an optimistic repetition rate of the laser system of 10 Hz this would translate into a treatment time of about 20 mins. The dose distributions obtained in our study for laser-driven protons show promising results, like the optimal plan displayed in figure 13, with high dose conformation and good sparing of surrounding organs at risk. The corresponding tumour coverage and conformity indexes of TC=98%, CN=87% are comparable to conventional clinically accepted treatment plans. In figure 14, the cumulative dose volume histogram (DVH) is shown for the planning target volume (PTV) as well as exemplary organs at risk and a ring structure around the tumour with a thickness of 1 cm. The DVH of the PTV shows a steep fall-off with $D_{2\%} = 2.09$ Gy and $D_{98\%} = 1.90$ Gy with good sparing of organs at risks (where $D_{2\%}$ and $D_{98\%}$ is the minimum dose received by at least 2% and 98% of the tumour volume, respectively).

4 Discussion and Outlook

The high-power laser-driven proton acceleration has captured the attention of both laser and medical physics communities for the size and cost reduction of PT facilities. Although, the milestone of accelerating protons to therapeutic proton energies, up to 250 MeV, is still to be reached, the recent results from ongoing research exhibit the prospects of laser-driven PT. On a side note, the use of heavier ions for radiation therapy, like He ion [52, 53], is gaining interests in the medical community because of their dosimetric and radio-biological benefits over proton beams. These beams can also be catered with the next generation laser development within the presented system. Nevertheless, to bring this technology to the clinics, it is necessary to develop the concepts and equipment to utilize laser-driven proton beams which are characterized by specific beam properties, like very short, ultra intense bunches with large energy spread, large divergence and low repetition rate. For example, these beams require full characterization for radio-biological effects [54, 55] for ultra-high dose rate regimes as they can reach up to 9 orders of magnitude higher dose-rates than conventional beams, and also specialized

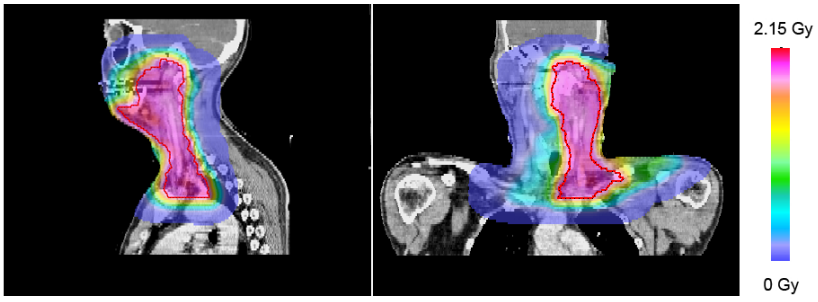

Figure 13: Dose distribution for the laser-driven proton plan generated with the pulsed LAP beams as per output parameters for the new gantry. A representative sagittal and axial view of the head and neck cancer patient shows the dose map per fraction to the planning target volume (PTV, red line) structure.

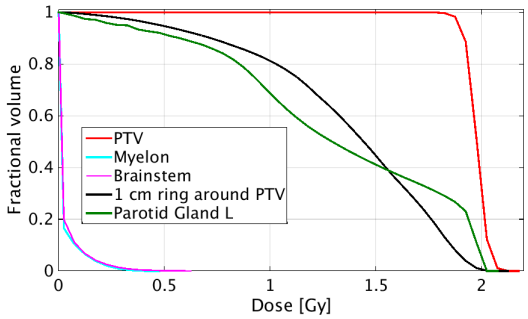

Figure 14: Cumulative dose-volume histogram (DVH) of the laser-driven proton plan. The prescribed dose per fraction to the planning target volume (PTV) is 2 Gy. The histogram for the 1 cm ring structure around the PTV is also shown which was used for dose optimization, as well as histograms for surrounding organs at risk. The myelon and the brainstem being the most critical organs, show only a maximum dose as low as 0.48 Gy and 0.6 Gy per fraction, respectively.

beam monitoring and dosimetry equipment for intense pulsed broad-energetic beams [56–61], along with the beam control and transport system.

In this paper, we have investigated how to control and deliver laser-driven proton beams and presented a new compact and light-weight isocentric gantry concept as a solution to bring laser-driven protons to the patient and to deliver a tumour conformal dose distribution. Due to the specific LAP beam properties, the presented gantry is integrated with multiple functionalities, i.e. integrated with capturing and energy selection systems with achromatic beam transport and a complete new and efficient dose delivery system, ELPIS. This presents a considerable improvement over the previous design, cf. [30], in terms of beam control, efficiency and mainly the dose delivery system as discussed in section 1.3. The presented gantry is also based on air-core pulse powered magnets, in contrast to conventionally utilized iron-core magnets in most proton therapy gantries. It is worthwhile to mention that abandoning the iron-core not only elevates the field strength but also makes pulsed magnets much lighter in weight, e.g. a 45° pulsed bending magnet with ~8 T field strength is about 60 times lighter than a 45° 2 T iron-core magnet. This in turn would lower the mechanical constraints on the support structures and the architecture of the therapy buildings.

Although the presented gantry design requires only three types of magnets namely solenoids, dipoles and quadrupoles, but pulsed magnets are challenging to design and construct. This is mainly because the magnetic field region of interest needs to be shaped via current carrying thick copper wires around an air-core, in contrast to the conventional magnets where the iron-core carries the magnetic-flux and the shape of the iron-core determines the magnetic field distribution. To realize the presented gantry concept, research and development of pulsed magnets is necessary and is in progress, as currently they are not readily available. The pulsed solenoid has been developed and its functionality for low energy laser-driven proton beams has been established in several experiments [41–43]. A first prototype of pulsed dipole bending magnet, i.e. 45° pulsed sector magnet, has been designed and manufactured [44, 45], which is currently being characterized. Furthermore, the first prototype pulsed quadrupole has been designed which is currently being manufactured [46]. The magnetic design and field values used in this gantry design are based on these experiences and are pragmatic.

The simulation results advocate that the presented gantry design has improved capture and transport efficiency, which is about 2-4 orders of magnitude higher than the low-acceptance beamline designs, c.f. [28, 62] and the maximum transport efficiency has been increased from 22% to 97% compared with the previous pulsed gantry [30]. The two step capture and collimation system provided a better beam control and a simpler design for the energy selection system. Furthermore, the beam can be controlled for smaller transverse dimensions for the new dose delivery, ELPIS system. The ELPIS system is designed to combine not only conventional dose delivery options in one equipment, but also could provide LAP bunches with a wide range of optimizable parameters, i.e. shape, size, axial length and lateral position, which can all be done simultaneously. Thus, there is no need to physically switch between scanning and scattering options. Furthermore, advanced dose delivery schemes, like axial and lateral clustering and partial volume irradiation can easily be implemented. It utilizes magnetic fields to shape the beam, in contrast to passive methods, thus conserves the number of protons for efficient dose delivery.

In our TPS study, we have found that with the assumed initial proton spectrum and with the improved transport efficiency the output LAP bunches have up to 2 orders of magnitude higher proton number per shot then necessary for a dose of 2 Gy per fraction even when applying beams with 2 cm spot size. This would give flexibility to the laser community for optimizing laser proton acceleration, i.e. reducing the number of protons per bunch while improving the stability of the beam in the future, and also provides a cushion for the small losses in transport efficiencies while including additional equipment like beam monitors in the gantry.

The feasibility of laser-driven PT would depend on the efficient use of the properties of LAP beams, i.e. large energy spread with variable beam sizes. Here it is worthwhile to mention that the main benefit would be the size and cost reduction of the PT facilities, if LAP beams could match the high standards in 3D tumour conformal dose delivery of the conventional PT. The TPS study demonstrated that the application of the axial clustering scheme could deliver clinically acceptable treatment plans, however, this would take about 1.5-2 times longer to deliver than conventional proton plans. Hofmann et al. [31] showed that if an intensity modulation scheme could be included, the 3D TPS LAP-CERR can optimize proton fluence delivery and a shot reduction of the order of few tens of percent can be achieved. This intensity modulation could be enabled easily in the presented gantry design via the introduction of physical scatterers between the capturing and collimating solenoids. Furthermore, the inclusion of other mentioned dose schemes, like partial volume irradiation ([49]), which can further optimize the efficiency in dose delivery by simultaneous axial and lateral clustering of spots and may further reduce the treatment time, which is an ongoing project. This would give more flexibility in 3D TPS as the dose delivery system, ELPIS, is fully capable to shape and deliver variable size beams with variable energy widths.

5 Conclusion

With the present development of petawatt class high-power laser systems, laser-driven proton acceleration on micrometer scale could be usable as compact proton sources with therapeutic energies up to 250 MeV. We have presented a pulse powered isocentric gantry design to control, transport and shape these laser-driven intense pulsed proton beams, along with demonstrating its clinical functionality. Our compact gantry design shows that there is a huge potential to reduce the size of PT facilities while maintaining the high treatment standards of existing facilities in tumour conformed dose delivery. The presented gantry functionality with the integrated new ELPIS system allows to deliver LAP beams by applying advanced treatment options, therefore, it is worthwhile to further develop 3D TPS, in particular for lateral clustering and partial volume irradiation schemes. Also, for gantry realization research and development of pulsed magnets and pulse power-supply is ongoing. It will take time to establish laser-driven PT as a clinical application, however, the development and progress is promising.

6 Acknowledgments

We would like to acknowledge and thank U. Lehnert, T. Herrmannsdörfer, M. Sobiella and B. Lutz from the Helmholtz-Zentrum Dresden-Rossendorf for the useful discussions. We also acknowledge the financial support by the German Ministry of Education and Research (BMBF), grant numbers 03ZIK445, 03Z1N511 and 03Z1O511, the DFG cluster of excellence Munich-Centre for Advanced Photonics and EC LASERLAB-EUROPE/LEPP contract number 654148.

References

[1] L Cozzi, A Fogliata, A Lomax, and A Bolsi. A treatment planning comparison of 3D conformal therapy, intensity modulated photon therapy and proton therapy for treatment of advanced head and neck tumours. *Radiother. Oncol.*, 61:287–297, 2001.

[2] H Paganetti, B S Athar, M Moteabbed, J A Adams, U Schneider, and T I Yock. Assessment of radiation-induced second cancer risks in proton therapy and imrt for organs inside the primary radiation field. *Phys. Med. Biol.*, 57(19):6047, 2012.

[3] M Moteabbed, T I Yock, and H Paganetti. The risk of radiation-induced second cancers in the high to medium dose region: a comparison between passive and scanned proton therapy, IMRT and VMAT for pediatric patients with brain tumors. *Phys. Med. Biol.*, 59(12):2883, 2014.

[4] D Meer and S Psoroulas. Gantries and dose delivery systems. *Mod. Phys. Lett. A*, 30(17):1540021, 2015.

[5] H Owen, A Lomax, and S Jolly. Current and future accelerator technologies for charged particle therapy. *Nucl. Instrum. Meth. A*, 809:96–104, 2016.

[6] A Smith, M Gillin, M Bues, X R Zhu, K Suzuki, R Mohan, S Woo, A Lee, R Komaki, J Cox, K Hiramoto, H Akiyama, T Ishida, T Sasaki, and K Matsuda. The M. D. Anderson proton therapy system. *Med. Phys.*, 36(9):4068–4083, 2009.

[7] PTCOG-Particle therapy facilities in operation (incl. patient statistics). http://ptcog.web.psi.ch/ptcentres.html, December 2015.

[8] D Trbojevic, B Parker, E Keil, and A M Sessler. Carbon/proton therapy: A novel gantry design. *Phys. Rev. ST Accel. Beams*, 10:053503, 2007.

[9] A Garonna, U Amaldi, R Bonomi, D Campo, A Degiovanni, M Garlasché, I Mondino, V Rizzoglio, and S V Andrés. Cyclinac medical accelerators using pulsed C^{6+}/H_2^+ ion sources. *J. Instrum.*, 5(09):C09004, 2010.

[10] H Daido, M Nishiuchi, and A S Pirozhkov. Review of laser-driven ion sources and their applications. *Rep. Prog. Phys.*, 75:056401, 2012.

[11] P M Hill, E E Klein, and C Bloch. Optimizing field patching in passively scattered proton therapy with the use of beam current modulation. *Phys. Med. Biol.*, 58(16):5527, 2013.

[12] A Zografos, C Hettler, Y Parker, M Moyers, D Pearson, V Joshkin, K Leung, F Huang, C Cohen-Jonathan, M Rougieri, T Brown, and R Hamm. Development of the dielectric wall accelerator. In *Proceedings, 4th International Particle Accelerator Conference (IPAC 2013), Shanghai, China*, 2013.

[13] K W D Ledingham, W Galster, and R Sauerbrey. Laser-driven proton oncology–a unique new cancer therapy? *Brit. J. Radiol.*, 80:855–858, 2007.

[14] V Malka, J Faure, Y A Gauduel, E Lefebvre, A Rousse, and K Ta Phuoc. Principles and applications of compact laser-plasma accelerators. *Nat. Phys.*, 4:447–453, 2008.

[15] International Committee for Future Accelerators, Beam Dynamics Newsletter no. 56:51-59, Iss. Eds.:W Leemans, W Chou, M Uesaka, Ed. in Chief: W Chou, December 2011.

[16] J. Schreiber, P. R. Bolton, and K. Parodi. Invited review article: hands-on laser-driven ion acceleration: A primer for laser-driven source development and potential applications. *Review of Scientific Instruments*, 87(7), 2016.

[17] M Roth, S Bedacht, S Busold, O Deppert, G Schaumann, F Wagner, A Terbartz, D Jung, D Schumacher, A Blazevic, V Bagnoud, F Kroll, T E Cowan, C Brabetz, K Falk, A Favalli, J Fernandez, C Gautier, C Hamilton, R P Johnson, K Schoenberg, T Shimada, G Wurden, M Geissel, and M Schollmeier. Breaking the 70 MeV proton energy threshold in laser proton acceleration and guiding beams to applications. In *Proceedings, 5th International Particle Accelerator Conference (IPAC 2014), Dresden, Germany*, June 2014.

[18] F Wagner, O Deppert, C Brabetz, P Fiala, A Kleinschmidt, P Poth, V A Schanz, A Tebartz, B Zielbauer, M Roth, T Stöhlker, and V Bagnoud. Maximum proton energy above 85 MeV from the relativistic interaction of laser pulses with micrometer thick CH_2 targets. *Phys. Rev. Lett.*, 116:205002, May 2016.

[19] T Kluge, T E Cowan, A Debus, U Schramm, K Zeil, and M Bussmann. Electron temperature scaling in laser interaction with solids. *Phys. Rev. Lett.*, 107(20):205003, 2011.

[20] T Kluge, W Enghardt, S D Kraft, U Schramm, K Zeil, T E Cowan, and M Bussmann. Enhanced laser ion acceleration from mass-limited foils. *Phys. Plasmas*, 17(12):123103, 2010.

[21] K Zeil, J Metzkes, T Kluge, M Bussmann, T E Cowan, S D Kraft, R Sauerbrey, B Schmidt, M Zier, and U Schramm. Robust energy enhancement of ultrashort pulse laser accelerated protons from reduced mass targets. *Plasma Physics and Controlled Fusion*, 56(8):084004, 2014.

[22] S Garcia, D Chatain, and J P Perin. Continuous production of a thin ribbon of solid hydrogen. *Laser Part. Beams*, 32:569–575, 12 2014.

[23] C Danson, D Hillier, N Hopps, and D Neely. Petawatt class lasers worldwide. *High Power Laser Science and Engineering*, 3, 2015.

[24] T E Cowan, J Fuchs, H Ruhl, A Kemp, P Audebert, M Roth, R Stephens, I Barton, A Blazevic, E Brambrink, J Cobble, J Fernández, J-C Gauthier, M Geissel, M Hegelich, J Kaae, S Karsch, G P Le Sage, S Letzring, M Manclossi, S Meyroneinc, A Newkirk, H Pépin, and N Renard-LeGalloudec. Ultralow emittance, multi-MeV proton beams from a laser virtual-cathode plasma accelerator. *Phys. Rev. Lett.*, 92:204801, May 2004.

[25] D Schardt, T Elsässer, and D Schulz-Ertner. Heavy-ion tumor therapy: Physical and radiobiological benefits. *Rev. Mod. Phys.*, 82:383–425, 2010.

[26] C M Ma, I Velchev, E Fourkal, J S Li, W Luo, J Fan, T Lin, and A Pollack. Development of a laser-driven proton accelerator for cancer therapy. *Laser Phys.*, 16(4):639–646, 2006.

[27] S Schell and J J Wilkens. Modifying proton fluence spectra to generate spread-out bragg peaks with laser accelerated proton beams. *Phys. Med. Biol.*, 54:N459–N466, 2009.

[28] J Fan, W Luo, E Fourkal, T Lin, J Li, I Veltchev, and C M Ma. Shielding design for a laser-accelerated proton therapy system. *Phys. Med. Biol.*, 52:3913–3930, 2007.

[29] S Faby and J J Wilkens. Assessment of secondary radiation and radiation protection in laser-driven proton therapy. *Z. Med. Phys.*, 25(2):112 – 122, 2015.

[30] U Masood, M Bussmann, TE Cowan, W Enghardt, L Karsch, F Kroll, U Schramm, and J Pawelke. A compact solution for ion beam therapy with laser accelerated protons. *Appl. Phys. B*, 117(1):41–52, October 2014.

[31] K M Hofmann, U Masood, J Pawelke, and J J Wilkens. A treatment planning study to assess the feasibility of laser-driven proton therapy using a compact gantry design. *Med. Phys.*, 42(9):5120–5129, 2015.

[32] R A Snavely, M H Key, S P Hatchett, T E Cowan, M Roth, T W Phillips, M A Stoyer, E A Henry, T C Sangster, M S Singh, S C Wilks, A MacKinnon, A Offenberger, D M Pennington, K Yauike, A B Langdon, B F Lasinski, M D Perry, and E M Campbell. Intense high-energy proton beams from petawatt-laser irradiation of solids. *Phys. Rev. Lett.*, 85(14):2945–2948, 2000.

[33] T Esirkepov, M Borghesi, S V Bulanov, G Mourou, and T Tajima. Highly efficient relativistic-ion generation in the laser-piston regime. *Phys. Rev. Lett.*, 92(17):175003, 2004.

[34] X Q Yan, H C Wu, Z M Sheng, J E Chen, and J Meyer-ter Vehn. Self-organizing GeV, nanocoulomb, collimated proton beam from laser foil interaction at $7 \times 10^{21}\, W/cm^2$. *Phys. Rev. Lett.*, 103(4):135001, 2009.

[35] L Yin, B J Albright, K J Bowers, D Jung, J C Fernández, and B M Hegelich. Three-dimensional dynamics of breakout afterburner ion acceleration using high-contrast short-pulse laser and nanoscale targets. *Phys. Rev. Lett.*, 107:045003, Jul 2011.

[36] B Qiao, S Kar, M Geissler, P Gibbon, M Zepf, and M Borghesi. Dominance of radiation pressure in ion acceleration with linearly polarized pulses at intensities of 10^{21} W cm^{-2}. *Phys. Rev. Lett.*, 108:115002, Mar 2012.

[37] B M Hegelich, I Pomerantz, L Yin, H C Wu, D Jung, B J Albright, D C Gautier, S Letzring, S Palaniyappan, R Shah, K Allinger, R Hrlein, J Schreiber, D Habs, J Blakeney, G Dyer, L Fuller, E Gaul, E Mccary, A R Meadows, C Wang, T Ditmire, and J C Fernandez. Laser-driven ion acceleration from relativistically transparent nanotargets. *New J. Phys.*, 15(8):085015, 2013.

[38] A Henig, S Steinke, M Schnürer, T Sokollik, R Hörlein, D Kiefer, D Jung, J Schreiber, B M Hegelich, X Q Yan, J Meyer-ter Vehn, T Tajima, P V Nickles, W Sandner, and D Habs. Radiation-pressure acceleration of ion beams driven by circularly polarized laser pulses. *Phys. Rev. Lett.*, 103:245003, Dec 2009.

[39] I Hofmann, J Meyer ter Vehn, X Yan, A Orzhekhovskaya, and S Yaramyshev. Collection and focusing of laser accelerated ion beams for therapy applications. *Phys. Rev. ST Accel. Beams*, 14:031304, 2011.

[40] I Hofmann, J Meyer ter Vehn, X Yan, and H Al-Omari. Chromatic energy filter and characterization of laser-accelerated proton beams for particle therapy. *Nucl. Instrum. Meth. A*, 681:44 – 54, 2012.

[41] T Burris-Mog, K Harres, F Nürnberg, S Busold, M Bussmann, O Deppert, G Hoffmeister, M Joost, M Sobiella, A Tauschwitz, B Zielbauer, V Bagnoud, T Hermannsdoerfer, M Roth, and T E Cowan. Laser accelerated protons captured and transported by a pulse power solenoid. *Phys. Rev. ST Accel. Beams*, 14:121301, 2011.

[42] S Busold, D Schumacher, O Deppert, C Brabetz, F Kroll, A Blažević, V Bagnoud, and M Roth. Commissioning of a compact laser-based proton beam line for high intensity bunches around 10 MeV. *Phys. Rev. ST Accel. Beams*, 17:031302, Mar 2014.

[43] S Busold, D Schumacher, C Brabetz, D Jahn, F Kroll, O Deppert, U Schramm, T E Cowan, A Blažević, V Bagnoud, and M Roth. Towards highest peak intensities for ultra-short MeV-range ion bunches. *Sci. Rep.*, 5(12459), 2015.

[44] M Schürer, T Hermannsdoerfer, L Karsch, F Kroll, U Masood, and J Pawelke. Advanced short-pulsed high-field electromagnetic dipoles for laser-based proton therapy. *Biomedical Engineering / Biomedizinische Technik*, 60(Suppl.1):284, 2015 September.

[45] M Schürer, L Karsch, J Pawelke, J Zschetzsche, and F Kroll. Elektromagnet zur Führung von Teilchenstrahlen zur Strahlentherapie. Germany, Patent No.: DE 10 2015 200 213, 2015.

[46] M Schürer, T Hermannsdoerfer, L Karsch, F Kroll, U Masood, M Sobiella, and J Pawelke. Entwicklung von Elektromagneten mit kurzen, hohen Strompulsen für die laserbasierte Protonentherapie. In *5. Dresdner Medizintechnik Symposium, Biomedizinische Technik von der Grundlagenforschung zum Transfer, Reports on Biomedical Engineering*, 2014.

[47] Helmut Wiedemann. *Particle Accelerator Physics*. Springer Verlag, 2007.

[48] Pulsar physics, Eindoven, The Netherlands. http://www.pulsar.nl/gpt/index.html, May 2013.

[49] S Schell and J J Wilkens. Advanced treatment planning methods for efficient radiation therapy with laser accelerated proton and ion beams. *Med. Phys.*, 37(10):5330–5340, 2010.

[50] Y Sun and C Adolphsen. Linac alignment algorithm: analysis on 1-to-1 steering. *SLAC-PUB-14323*.

[51] N J Lomax and S G Scheib. Quantifying the degree of conformity in radiosurgery treatment planning. *Int. J. Radiat. Oncol. Biol. Phys.*, 55(5):1409–1419, 2003.

[52] H Fuchs, M Alber, T Schreiner, and D Georg. Implementation of spot scanning dose optimization and dose calculation for helium ions in hyperion. *Med. Phys.*, 42(9):5157–5166, 2015.

[53] A Mairani, I Dokic, G Magro, T Tessonnier, F Kamp, D J Carlson, M Ciocca, F Cerutti, P R Sala, A Ferrari, T T Bhlen, O Jkel, K Parodi, J Debus, A Abdollahi, and T Haberer. Biologically optimized helium ion plans: calculation approach and its in vitro validation. *Phys. Med. Biol.*, 61(11):4283, 2016.

[54] K Zeil, M Bussmann, E Beyreuther, T Burris-Mog, T E Cowan, W Enghardt, L Karsch, S D Kraft, L Laschinsky, J Metzkes, D Naumburger, M Oppelt, C Richter, R Sauerbrey, M Schürer, U Schramm, and J Pawelke. Dose-controlled irradiation of cancer cells with laser-accelerated proton pulses. *Appl. Phys. B*, 110(4):437–444, 2012.

[55] K Brüchner, E Beyreuther, M Baumann, M Krause, M Oppelt, and J Pawelke. Establishment of a small animal tumour model for in vivo studies with low energy laser accelerated particles. *Radiation Oncology*, 9(1):1–9, 2014.

[56] C Richter, L Karsch, Y Dammene, S D Kraft, J Metzkes, U Schramm, M Schürer, M Sobiella, A Weber, K Zeil, and J Pawelke. A dosimetric system for quantitative cell irradiation experiments with laser-accelerated protons. *Phys. Med. Biol.*, 56:1529–1543, 2011.

[57] J Metzkes, L Karsch, S D Kraft, J Pawelke, C Richter, M Schürer, M Sobiella, N Stiller, K Zeil, and U Schramm. A scintillator-based online detector for the angularly resolved measurement of laser-accelerated proton spectra. *Rev. Sci. Instrum.*, 83:123301, 2012.

[58] L Karsch, C Richter, and J Pawelke. Experimental investigation of the collection efficiency of a ptw roos ionization chamber irradiated with pulsed beams at high pulse dose with different pulse lengths. *Z. Med. Phys.*, 21(1):4, 2011.

[59] F Kroll, J Pawelke, and L Karsch. Preliminary investigations on the determination of three-dimensional dose distributions using scintillator blocks and optical tomography. *Med. Phys.*, 40(8), 2013.

[60] L Karsch and J Pawelke. Theoretical investigation of the saturation correction for ionization chambers irradiated with pulsed beams of arbitrary pulse length. *Z. Med. Phys.*, 3:201–10, 2014.

[61] J Metzkes, K Zeil, S D Kraft, L Karsch, M Sobiella, M Rehwald, L Obst, H P Schlenvoigt, and U Schramm. An online, energy-resolving beam profile detector for laser-driven proton beams. *Rev. Sci. Instrum.*, 87(8), 2016.

[62] G A P Cirrone, M Carpinelli, G Cuttone, S Gammino, S B Jia, G Korn, M Maggiore, L Manti, D Margarone, J Prokupek, M Renis, F Romano, F Schillaci, B Tomasello, L Torrisi, A Tramontana, and A Velyhan. Elimed, future hadrontherapy applications of laser-accelerated beams. *Nucl. Instrum. Meth. A*, 730:174 – 177, 2013.